



Spectral response properties of higher visual neurons in *Drosophila melanogaster*

Taro Yonekura¹ · Junji Yamauchi¹ · Takako Morimoto¹ · Yoichi Seki¹

Received: 1 September 2019 / Revised: 27 November 2019 / Accepted: 29 November 2019 / Published online: 13 December 2019
© Springer-Verlag GmbH Germany, part of Springer Nature 2019

Abstract

The fruit fly *Drosophila melanogaster* can process chromatic information for true color vision and spectral preference. Spectral information is initially detected by a few distinct photoreceptor channels with different spectral sensitivities and is processed through the visual circuit. The neuroanatomical bases of the circuit are emerging. However, only little information is available in chromatic response properties of higher visual neurons from this important model organism. We used in vivo whole-cell patch-clamp recordings in response to monochromatic light stimuli ranging from 300 to 650 nm with 25-nm steps. We characterized the chromatic response of 33 higher visual neurons, including their general response type and their wavelength tuning. Color-opponent-type responses that had been typically observed in primates and bees were not identified. Instead, the majority of neurons showed excitatory responses to broadband wavelengths. The UV (300–375 nm) and middle wavelength (425–575 nm) ranges could be separated at the population level owing to neurons that preferentially responded to a specific wavelength range. Our results provide a first mapping of chromatic information processing in higher visual neurons of *D. melanogaster* that is a suitable model for exploring how color-opponent neural mechanisms are implemented in the visual circuits.

Keywords Color vision · Optic lobe · Color opponency · Color coding · Insect brain

Introduction

Color vision is widespread across the animal kingdom from mammals (especially primates), fishes, amphibians, birds, and crustaceans, to insects (Kelber et al. 2003). Color is perceived based on the activities of a few types of photoreceptors that have distinct spectral sensitivities. For true color vision, as one type of photoreceptor cannot differentiate wavelength and intensity, more than two types of photoreceptor inputs need to be compared to discriminate different light wavelengths independently of intensity (Kelber 2016). In contrast, spectral preference, which is a

wavelength-specific behavior, depends on light intensity and can be directly linked to a specific type or types of photoreceptors (Song and Lee 2018).

Fundamental knowledge of the neural mechanisms for color vision has mainly derived from primate studies (Gegenfurtner and Kiper 2003; Conway et al. 2010). Primates including humans possess trichromatic color vision based on three classes of photoreceptors denoted as long (L), middle (M), and short (S) wavelength sensitive photoreceptors. This initial photoreceptor tuning is transformed through the retinal circuits, where color-opponent neurons that are excited at one wavelength and inhibited at another emerge. The information is then further sent to the visual cortex via the lateral geniculate nucleus (Dacey and Packer 2003; Solomon and Lennie 2007). There are well-characterized two color-opponent axes; L vs M (red–green) and S vs (L + M) (blue–yellow). Additionally, these physiological properties account for the previously demonstrated psychological perception of colors: exclusive sensations for red–green and blue–yellow (Krauskopf et al. 1982; Gegenfurtner and Kiper 2003). Color information is further processed through the primary visual cortex to the extra striate cortex, e.g., blobs

Electronic supplementary material The online version of this article (<https://doi.org/10.1007/s00359-019-01391-9>) contains supplementary material, which is available to authorized users.

✉ Yoichi Seki
yseki@toyaku.ac.jp

¹ Laboratory of Molecular Neuroscience and Neurology, School of Life Sciences, Tokyo University of Pharmacy and Life Sciences, 1432-1 Horinouchi, Hachioji, Tokyo 192-0392, Japan

in V1 → thin stripes in V2 → globs in V4 → the inferior temporal cortex. However, color information processing in the higher brain centers is still largely unknown.

In insects, color vision studies were primarily performed in flower-visiting pollinators, such as bees and butterflies (Menzel and Backhaus 1989; Arikawa and Stavenga 2014; Hempel de Ibarra et al. 2014; Kinoshita and Arikawa 2014). Spectral sensitivities of photoreceptors have been characterized in detail. In particular, butterflies have expanded photoreceptor variations through opsin modifications and screening pigments (Arikawa and Stavenga 2014). Higher color vision processing, such as color constancy and color contrast, has been demonstrated in both insect groups (Neumeyer 1980, 1981; Kinoshita and Arikawa 2000; Kinoshita et al. 2008). Moreover, visual processing studies in honey bees have revealed trichromatic processing similar to humans (Menzel and Backhaus 1989). The primary visual

processing center is called the optic lobe, and consists of the lamina, medulla, and lobula complex (Fig. 1a). The lobula complex is divided into the lobula and lobula plate in dipterans and lepidopterans but fused in hymenopterans. In bees, the chromatic properties of medulla, lobula, and higher brain neurons have been examined by intracellular recordings, leading to the descriptions of various types of broadband neurons, narrowband neurons, and color-opponent neurons (Erber and Menzel 1977; Kien and Menzel 1977a, b; Hertel 1980; Riehle 1981; Hertel and Maronde 1987; Yang et al. 2004; Paulk et al. 2008, 2009a, b). However, how those chromatic and achromatic neurons construct the neural circuits for color vision remains to be determined.

D. melanogaster is an emerging model for studying the circuit bases of color processing mechanisms (Behnia and Desplan 2015) because of the vast knowledge on the neuroanatomical basis of the visual pathway (Fischbach and

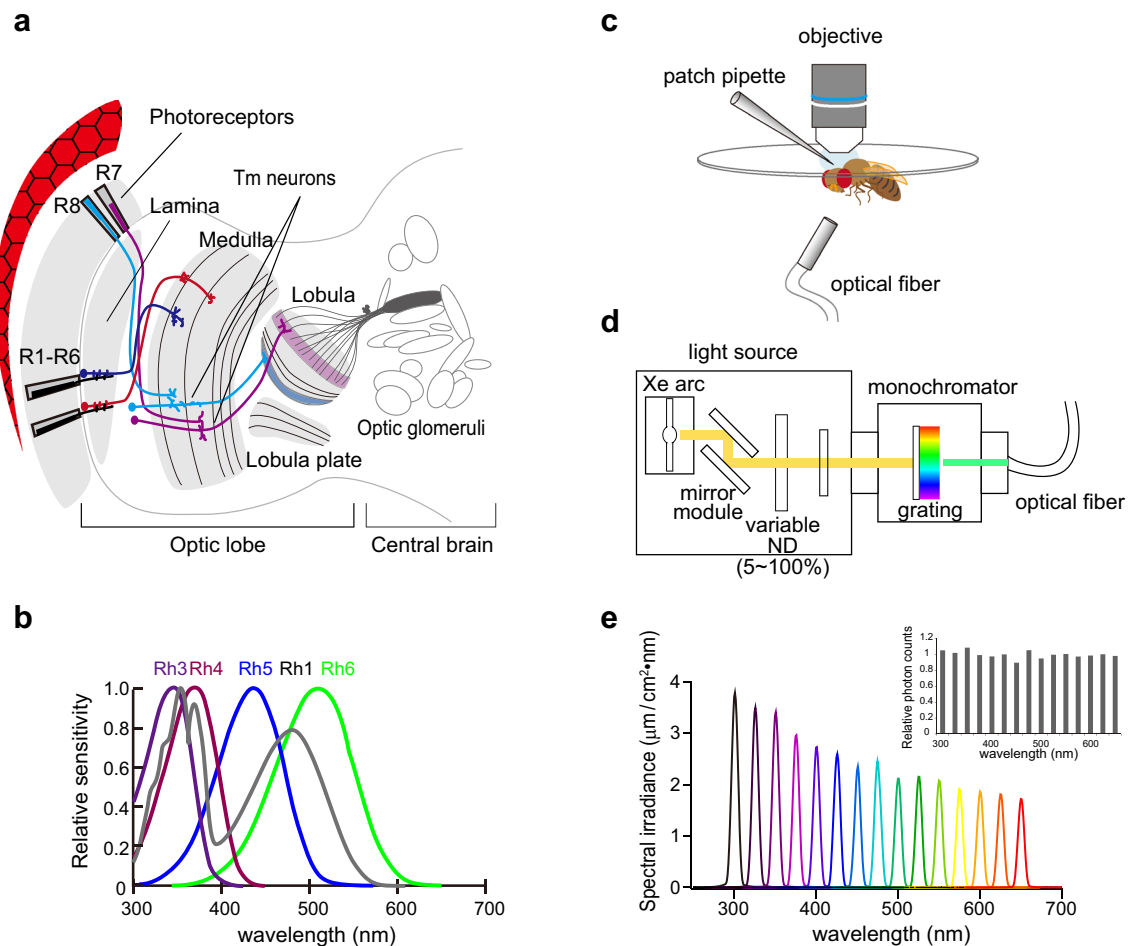


Fig. 1 Experimental setup for in vivo whole-cell path-clamp recording. **a** Schematic diagram of the *Drosophila* visual pathway from the periphery to higher brain centers. **b** Spectral sensitivities of the five rhodopsin types in *D. melanogaster*. (Adapted from Yamaguchi et al. 2010) **c** Schematic diagram of a fly preparation for in vivo whole-cell patch-clamp recording. **d** Schematic diagram of the light stimu-

lus apparatus consisting of a 300 W xenon lamp house and monochromator. ND, neutral density filter. **e** Spectral irradiance for each wavelength stimulus. The peak irradiance for each wavelength was adjusted inversely to the wavelength value (λ), so that photon numbers of each stimulus were approximately equivalent. Relative photon counts are shown in the inset

Dittrich 1989; Otsuna and Ito 2006; Takemura et al. 2013), the availability of circuit manipulation with rich genetic tools (Venken et al. 2011), and the true color vision ability demonstrated in flies by color memory tasks (Salomon and Spatz 1983; Schnaitmann et al. 2013; Melnattur et al. 2014) and spectral preference in phototaxis (Hu and Stark 1977; Jacob et al. 1977; Fischbach 1979; Gao et al. 2008; Yamaguchi et al. 2010; Otsuna et al. 2014). The compound eye of *D. melanogaster* consists of about 750 ommatidia, except for the dorsal rim area, stochastically distributed into two types (Wernet et al. 2006, 2015; Behnia and Desplan 2015). Pale ommatidia contain R7 photoreceptors expressing short UV-sensitive Rh3 opsins and R8 photoreceptors expressing blue-sensitive Rh5 opsins, whereas yellow ommatidia contain R7 photoreceptors expressing long UV-sensitive Rh4 opsins and R8 photoreceptors expressing green-sensitive Rh6 opsins (Fig. 1b) (Salcedo et al. 1999). As an exception, both Rh3 and Rh4 are co-expressed in R7s of yellow ommatidia in the dorsal third of the eye (Mazzoni et al. 2008). In addition to the four classes of inner photoreceptors, outer photoreceptors R1–6 express broadly tuned Rh1 opsins. The neuroanatomical organization of the optic lobes has been intensively characterized (Fischbach and Dittrich 1989). R7 and R8 photoreceptor neurons project their axons to the layers 6 and 3 of the medulla, respectively, whereas R1–6 photoreceptor neurons terminate in the lamina (Fischbach and Dittrich 1989; Takemura et al. 2008). Chromatic information is likely relayed via transmedulla (Tm) neurons to the lobula (candidates are Tm5a, b, c, Tm9, and Tm20) (Gao et al. 2008; Morante and Desplan 2008; Melnattur et al. 2014) and Tmy neurons to the lobula and lobula plate (candidates are Rh3-, Rh4-, Rh5-, and Rh6-Tmy) (Jagadeish et al. 2014). The information is further sent to higher brain centers, such as the lateral protocerebrum and optic glomeruli, via lobula columnar neurons and lobula tangential neurons (Otsuna and Ito 2006; Lin et al. 2016). However, the electrophysiological properties of these neurons are almost completely unknown, with the exception of the γ D-Kenyon cells (KCs) receiving the direct input from the medulla that contributes to the blue–green color discrimination task (Vogt et al. 2016). A recent study provided new insights for understanding the *Drosophila* color vision system by demonstrating the color-opponent mechanism of mutual inhibition between the axon terminals of the photoreceptors within the same ommatidia (Schnaitmann et al. 2018). However, how this initial color-opponent processing is transformed through the optic lobe visual circuit and transferred to the higher visual centers remains unknown.

In this study, we used in vivo whole-cell patch-clamp recordings to characterize the chromatic response properties of higher visual neurons in *D. melanogaster*. We robustly characterized the physiological responses of 33 neurons from putative third- or fourth-order interneurons that responded to

visual stimuli. We identified various response patterns by the difference in excitatory–inhibitory and ON–OFF temporal response components. Spectral properties of these neurons were characterized: the majority of neurons responded to broadband wavelengths, and a wavelength separation was found between the UV range (300–375 nm) and middle wavelength range (425–575 nm) by population level. Our results provide a first step toward understanding the central processing mechanism for color vision in *D. melanogaster*.

Materials and methods

Fly stocks

Flies were maintained on conventional medium under a 12-h light/12-h dark cycle at 24 °C. Adult females 1–3 days after eclosion were used in all experiments. Fly lines used in this study were Canton-S.

In vivo whole-cell patch-clamp recording

Patch-clamp recordings were performed with a configuration similar to that previously described (Suzuki et al. 2015). Flies were anesthetized in a plastic vial on ice for ~5 min and then gently inserted into a hole on a stretched Parafilm attached to the center of the recording chamber. The dorsal side of the thorax protruded through the hole above the film, whereas the head was bent down under the film. Then, the backside of the head was exposed by ripping the Parafilm to the edge of the head capsule. The gap between the Parafilm and head capsule or thorax was filled with two-component silicone (KWIK-SIL, WPI, Sarasota, FL, USA). The dorsal side of the film was immersed in saline (130 mM NaCl, 5 mM KCl, 2 mM MgCl₂, 2 mM CaCl₂, 36 mM sucrose, and 5 mM 4-(2-hydroxyethyl)-1-piperazineethanesulfonic acid [HEPES], pH 7.3). A window was cut in the backside of the head. Muscles and trachea were carefully removed using forceps to expose the target brain region. To remove the neurolemma, collagenase (1.5 mg/mL, Yakult, Tokyo, Japan) dissolved in extracellular saline was applied locally over the region between the optic lobe and central brain with a micropipette using positive pressure for approximately 5 min. Cell bodies exposed around the target region were visualized under an infrared differential interference contrast microscope (E600FN, Nikon, Tokyo, Japan) with a 40× water immersion objective (Fluor 40×, NA=0.80, WD=2.0 mm, Nikon). A CCD camera (ORCA-Flash4.0 or HiSCA C6790, Hamamatsu Photonics, Hamamatsu, Japan) was used to monitor the recording region. Whole-cell recording was made from a cell body with a glass pipette (8–14 M Ω) containing the internal solution: 140 mM potassium aspartate, 10 mM HEPES, 1 mM KCl, 4 mM Mg-ATP, 0.5 mM

Na₃GTP, 1 mM ethylene glycol-*bis*(β-aminoethyl ether)-*N,N,N',N'*-tetraacetic acid (EGTA) with or without 7 mM biocytin, pH 7.3. The membrane potential was recorded in current-clamp mode using an amplifier (MultiClamp 700B, Molecular Devices, CA, USA) with pCLAMP 9 software. Voltage recordings were sampled at 10 kHz. After break-in, the membrane potential was kept around –50 mV when injecting a small current, if necessary.

Light stimuli

Monochromatic light stimuli were provided by a 300 W xenon lamp house (MAX-303, Asahi Spectra, Tokyo, Japan) through a monochromator (CMS-100, Asahi Spectra). One-second monochromatic light (300–650 nm at 25 nm steps) was presented at 15-s interstimulus intervals. Thus, the whole set of stimuli consisted of 255 s. Spectral irradiance of each monochromatic stimulus was measured using a spectrometer (HSU-100S, Asahi Spectra) and the peak irradiance for each wavelength was adjusted inversely to the wavelength value (λ), so that photon numbers of each stimulus were approximately equivalent (Fig. 1e). The mean value of the photon counts of all the wavelength stimuli was $5.35 \times 10^{13} \pm 2.42 \times 10^{12}$ (photons/cm² s, \pm SD) (Fig. 1e). The whole set of stimuli was repeated several times by alternating ascending (300–650 nm) and descending (650–300 nm) orders, according to the conventional method used for measuring spectral responses of photoreceptors (e.g., Arikawa et al. 2003). We could not find any qualitative differences in the responses to these two different orders. The stimulus protocols were written with Python software and the light stimulus apparatus was controlled by Raspberry Pi (<https://www.raspberrypi.org/>). Light pulses were presented to the whole compound eye ipsilateral to the recording side through a quartz fiber. The end of the fiber (diameter = 5 mm) was placed 15 mm from the fly. The emitting light diffused across the broad area covering the entire body of the fly, so that the contralateral side of the compound eye was also illuminated.

Immunocytochemistry

For some preparations, staining of the recorded neuron was attempted with biocytin in the pipette. The following procedure was performed for those preparations. To visualize the brain regions, nc82 immunostainings were performed as previously described (Seki et al. 2010). Brains were fixed in 4% paraformaldehyde in phosphate-buffered solution (PBS; 0.1 M, pH 7.4) containing 0.2% Triton X-100 (PBST) for 30 min on ice. Then, the brains were washed with PBST for 60 min (3 times for 20 min) at room temperature (RT). After being blocked in 5% normal goat serum (NGS) in PBST (PBST-NGS) for 60 min at RT, the brains were incubated in

1:30 mouse monoclonal nc82 antibody [the Developmental Studies Hybridoma Bank (DSHB)] in PBST-NGS for 2 days at 4 °C. Then, the brains were washed for 60 min at RT and incubated in 1:200 goat anti-mouse Alexa Fluor 633 (A21052, Invitrogen) for 2 days at 4 °C. Afterwards, brains were washed again for 60 min and mounted in 80% glycerol. Additionally, biocytin-injected neurons were labeled with (1:500) Alexa Fluor 555 streptavidin (S-32355, Invitrogen), which was incubated with the secondary antibody for nc82, (1:200) goat anti-mouse Alexa Fluor 633 (A21052, Invitrogen). Images were obtained with a confocal microscope using a 40× objective (FV1200 or FV1000, Olympus, Tokyo, Japan). Three-dimensional reconstructions of a neuron and brain regions were performed with Amira 5.6 software.

Data analysis

Recording data were analyzed in Igor Pro (WaveMetrics, Lake Oswego, OR, USA) and MATLAB (The MathWorks, Natick, MA, USA) using custom software.

Spike extraction: Spike times were extracted from raw voltage traces as described in (Wilson et al. 2004), using an automated routine to detect minima in the second differential of the membrane potential. Manual corrections were added when necessary.

Response intensity: neuron's responses were evaluated using spike numbers during the 1-s light stimulus for ON response and the 1 s after the stimulus for OFF response. Spike numbers used for the analysis were obtained by subtracting the baseline frequencies calculated by averaging spike frequencies for 5 s before light ON stimuli. The mean response amplitude was calculated by averaging responses to repeated whole set of stimuli for each wavelength. In the four recordings (ON-OFF_1, ON_1, ON_2, and Inhibitory_1 neurons), stimulus duration was set for 1.2 s. These data were compensated when calculating ON and OFF responses using 0–1 s as ON phase and 1.2–2.2 s as OFF phase and excluding responses in 1–1.2 s for the analysis.

Lifetime sparseness: lifetime sparseness was calculated to quantify the selectivity of a neuron's spectral response profile (Willmore and Tolhurst 2001; Wilson et al. 2004):

$$S = \left(\frac{1}{1 - \frac{1}{N}} \right) \left(1 - \frac{\left(\sum_{j=1}^N r_j / N \right)^2}{\sum_{j=1}^N r_j^2 / N} \right),$$

where N is number of wavelengths (15 in this study), and r_j is response intensity of the neuron to wavelength j . Any values of $r_j < 0$ were set to zero before computing lifetime sparseness. S varies between 0 (broadly tuned) and 1 (narrowly tuned), where 0 represents a flat tuning curve and 1 corresponds to just one non-zero response.

Hierarchical cluster analysis and principal component analysis (PCA) were performed using MATLAB. Hierarchical cluster analysis was performed using correlation distance and Ward's classification method. PCA was performed based on the response intensity of 25 neurons for ON and OFF responses to 15 wavelengths. Representations of 15 wavelengths were plotted in the two-dimensional space as PC1 and PC2 for each axis. Spike frequency values were transformed to *z*-score values before the PCA analysis. *k*-means clustering was performed with Paleontological STatistics (PAST) software (<https://folk.uio.no/ohammer/past/>).

Results

To examine light response properties of higher visual neurons and their dependence on spectral differences, whole-cell patch-clamp recordings were performed *in vivo* from randomly targeted cell bodies residing between the optic lobe and central brain at the posterior surface of the brain. To characterize the spectral response pattern of the neurons, the eyes of flies were stimulated with various wavelengths of photon number-adjusted monochromatic light ranging from 300 to 650 nm with 25 nm steps (Fig. 1c–e). In total, we successfully recorded 46 neurons. We excluded neurons that responded with attenuated spike firings or with non-spiking slow membrane potential deflection from further analysis and focused on 33 neurons that reliably showed spike firings. These neurons were tested with the whole set of wavelength stimuli 2–6 times (mean = $3.76 \pm \text{SD} = 1.26$; see “Materials and methods”). We characterized general response patterns, spectral tuning properties, and separation of wavelength information at the population level of the neurons.

Classification of neurons based on typical response patterns

We characterized general response patterns of recorded neurons based on response polarity (excitatory or inhibitory) and response timing (at stimulus ON or OFF). Light stimuli were applied for 1 s and the interval between stimuli was 15 s. We repeated the whole set of stimuli several times in alternating ascending order (stimuli from 300 to 650 nm) and descending order (650–300 nm) with 25-nm steps. We classified the 33 light-responsive neurons based

on the three typical response patterns to light stimuli that were consistently observed, mostly independent of stimulus wavelengths (Table 1). The neurons that showed excitatory responses (increased spike frequency) were categorized into two types: an excitatory ON–OFF type showing excitatory responses both at light ON and light OFF (Fig. 2) and an excitatory ON type showing excitatory responses only at light ON (Fig. 3). The third type was named inhibitory type and displayed an inhibitory response at light ON (Fig. 4). A few neurons were categorized as extra, because they showed light responses but following an inconsistent pattern in repeated stimuli. In this section, we focused our analysis on the temporal components of the response instead of the different response patterns to different light wavelengths. Most of the recorded neurons retained relatively consistent general response patterns for the most induced responses (see below and Supplemental Fig. 1). The properties of spectral tuning are addressed in detail later in the section ‘Wavelength tuning of higher visual neurons’.

Excitatory ON–OFF response type

The neurons that showed a spike firing increase during the light ON phase and after the onset of light OFF were classified as excitatory ON–OFF type ($n = 20$, Fig. 2, Table 1). Spike firing frequency usually reached a peak in 50–150 ms after the onset of light ON or OFF. Variations were found in the duration of firing after the peak. For example, some neurons kept spike firing during ON stimuli with a slow decline of firing frequency (phasic–tonic; Fig. 2a, c), whereas others ceased firing rapidly within a short period during ON stimuli (phasic; Fig. 2b, d). OFF response had a similar variation to the ON response, where some neurons showed only phasic spike firing immediately at the offset of stimuli (Fig. 2a, c, d), whereas others displayed phasic–tonic responses (Fig. 2b). Two neurons showed an off-peak of spike firing at the offset of stimuli, but the membrane potential started rising slightly before the light OFF (Fig. 2d). This rise might be caused by a rebound to the onset burst firing, but the mechanism was not addressed in this study.

Excitatory ON response type

The neurons that showed a spike firing increase during the light ON phase and no clear spike firing increase at the

Table 1 Classification of neurons by general response patterns

Response types	<i>n</i>	Descriptions of variations
Excitatory ON–OFF	20	Phasic-tonic or phasic excitation at ON and OFF response
Excitatory ON	8	Phasic-tonic or phasic excitation at ON response
Inhibitory	2	Tonic or phasic inhibition at ON response followed by excitation
Extra	3	Excitation and/or inhibition with low reproducibility

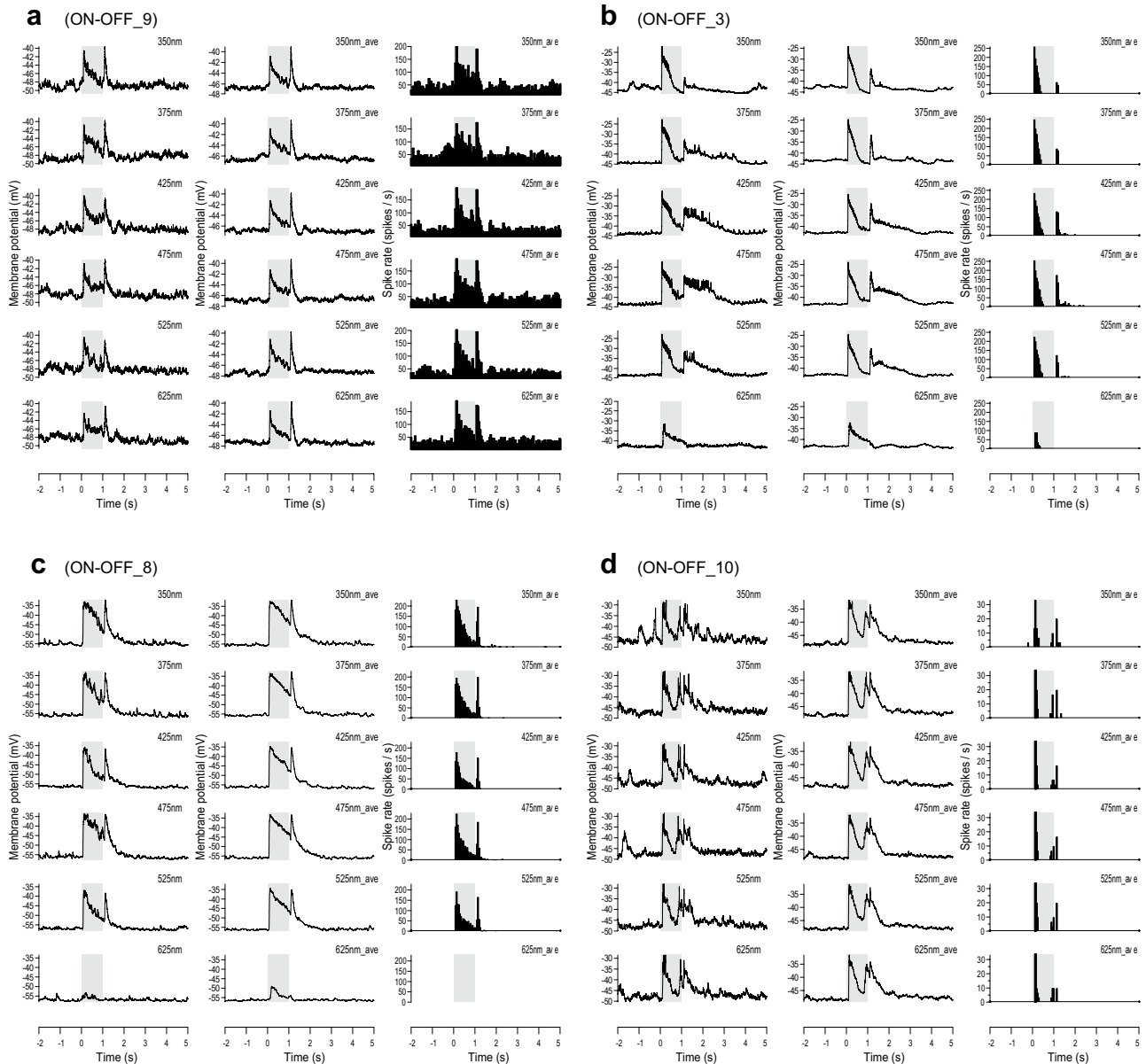
Excitatory ON–OFF type ($n = 20$)

Fig. 2 Excitatory ON–OFF response type. **a** Left column: Example traces of light responses of an excitatory ON–OFF type neuron (ON–OFF_9) to the six wavelength stimuli (350, 375, 425, 475, 525, 625 nm). Center column: Average membrane potential traces of the responses to four repeated stimulus sets. Right column: average peristimulus time histograms (PSTHs) with 50 ms time bins of the four repeated stimulus sets. **b–d** Response patterns of three other ON–OFF

type neurons [ON–OFF_3(b), ON–OFF_8(c), ON–OFF_10(d)] shown in the same configuration as in **a**. Note that (in **d**) the membrane potential started rising slightly before the light OFF and there is a tiny gap in spike firings at the light OFF. Average membrane potential traces and PSTHs are calculated with the responses to four (**b**) and six (**c**, **d**) repeated stimulus sets. Full traces to all wavelength stimuli are shown in Supplemental Fig. 1

offset of stimuli were classified as excitatory ON type ($n = 8$; Fig. 3, Table 1). Typically, spike firing peaked in 50–150 ms after the onset of light ON. We found two variations in the duration of firing similar to the excitatory ON–OFF type. Some neurons showed phasic–tonic responses in which spike firing continued after the peak with a slow decline during ON stimuli or even after the offset of stimuli (Fig. 3a),

whereas others displayed phasic responses in which spike firing ceased rapidly after the onset of stimuli (Fig. 3b).

Inhibitory response type

The neurons that displayed a substantial inhibitory phase (ceased firing and hyperpolarizing membrane deflection)

Excitatory ON type (n = 8)

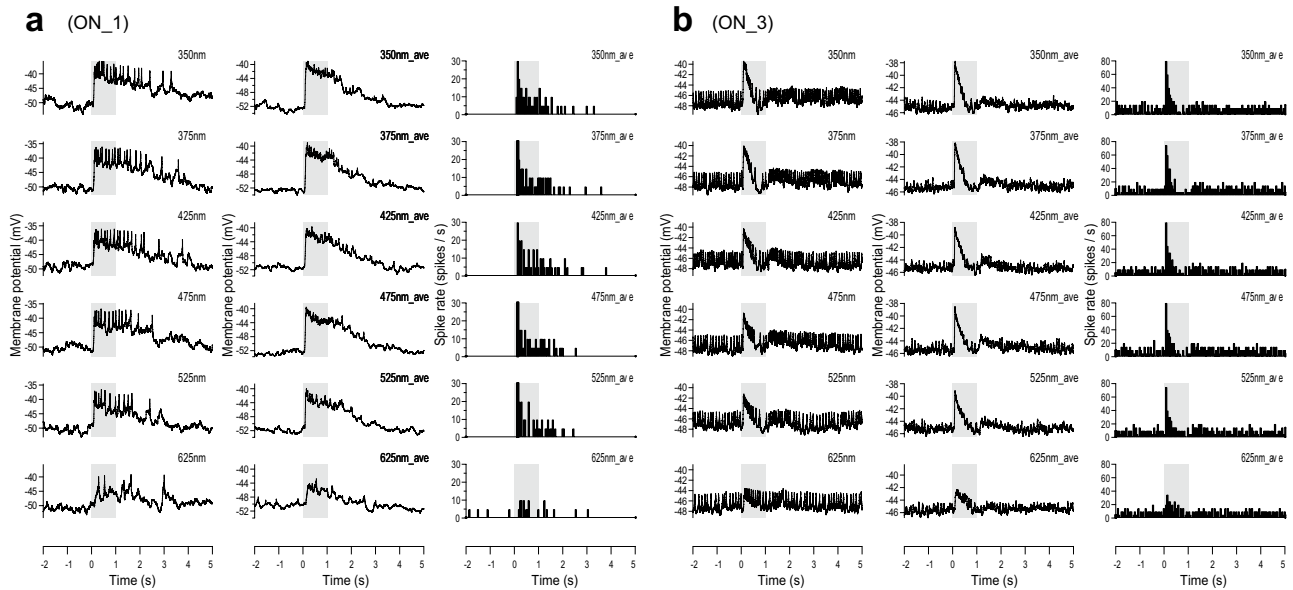


Fig. 3 Excitatory ON response type. **a** Left column: Example traces of light responses of an excitatory ON type neuron (ON_1) to the six wavelength stimuli (350, 375, 425, 475, 525, 625 nm). Center column: Average membrane potential traces of the responses to four repeated stimulus sets. Right column: average PSTHs with 50 ms

time bins of the four repeated stimulus sets. **b** Response pattern of other ON type neuron (ON_3) shown in the same configuration as in **a**. Average membrane potential traces and PSTHs are calculated with the responses to four repeated stimulus sets. Full traces to all wavelength stimuli are shown in Supplemental Fig. 1

Inhibitory type (n = 2)

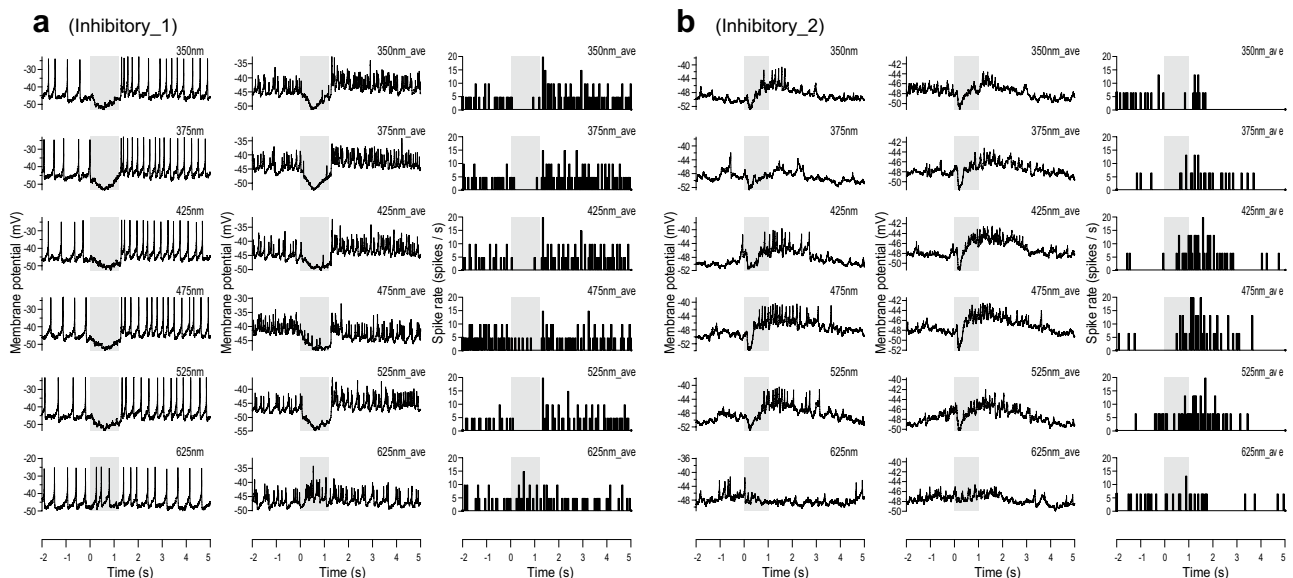


Fig. 4 Inhibitory response type. **a** Left column: Example traces of light responses of an inhibitory type neuron (Inhibitory_1) to the six wavelength stimuli (350, 375, 425, 475, 525, 625 nm). Center column: Average membrane potential traces of the responses to three repeated stimulus sets. Right column: average PSTHs with 50 ms

time bins of the four repeated stimulus sets. **b** Response pattern of the other Inhibitory type neuron (Inhibitory_2) shown in the same configuration as in **a**. Average membrane potential traces and PSTHs are calculated with the responses to three repeated stimulus sets. Full traces to all wavelength stimuli are shown in Supplemental Fig. 1

during the light ON response were classified as inhibitory type ($n=2$; Fig. 4, Table 1). One neuron showed tonic inhibitory response during light ON stimuli and a slight spike firing increase after the stimulus offset (Fig. 4a). Interestingly, this neuron displayed small excitatory responses to longer wavelength stimuli (~ 625 nm; Fig. 4a, see below for further information). The other neuron showed a phasic inhibitory response after light ON and a tonic firing increase following the inhibition (Fig. 4b). Although we named it the inhibitory response type, the inhibitory phases are followed by excitatory phases, and the total response of this type of neurons may not be necessarily inhibitory.

Extra types

The neurons that showed excitatory and/or inhibitory responses to light stimuli but inconsistently in repeated stimuli were classified as extra types ($n=3$; Table 1, Supplemental Fig. 1). For example, one neuron displayed inhibitory responses to a few wavelength stimuli in the first round of the stimulus set, but did not show the same pattern in the other round of the stimulus set (extra_2, Supplemental Fig. 1). These neurons could be miscategorized into color opponent if the recording is performed only for a single stimulus. This kind of neurons might be associated with light-induced flexible behaviors and not belong to pathways of visual perception, causing inconsistent responses.

We quantitatively evaluated our classification of response types by cluster analysis based on the time course of firing frequency change during the light ON and OFF phases of the 28 recorded neurons (Five neurons whose spike timing could not be reliably extracted by our algorithm were excluded. They were all excitatory ON–OFF type.). First, we reconstructed typical response patterns for each neuron using averaged peristimulus time histogram (PSTH) with 200 ms bins from the onset of the stimulus ($t=0$ s) to 1 s after the offset of the stimulus ($t=2$ s). Responses to several represented wavelengths were picked up for average histograms (Fig. 5a). We selected 350, 375, 425, 475, and 525 nm, which are close to each photoreceptor's peak sensitivities, and as shown in the next section, most neurons showed their typical responses to these wavelengths. We applied cluster analysis based on correlation distances of the typical response pattern for each neuron (ten bins in the PSTH from 0 to 2 s) (Fig. 5b). The hierarchical tree reveals that inhibitory types are separated with two extra types in the first cluster (Fig. 5b, c). Some of the excitatory ON–OFF types are separated from other types in the second cluster (Fig. 5b, c). Excitatory ON types are separated, but largely intermingled with other excitatory ON–OFF types in the third cluster (Fig. 5b, c). This separation could be accounted for by the shape of the PSTH: the neurons in the first cluster tend to have an $\text{ON} < \text{OFF}$ response amplitude, the neurons

in the second cluster showed $\text{ON} = \text{OFF}$, and those in the third cluster tend to show $\text{ON} > \text{OFF}$ (Fig. 5a). These results suggest that some of the ON–OFF and ON response type neurons represent likely a continuum in terms of quantitative spike frequency change during the time course of their typical responses.

Wavelength tuning of higher visual neurons

In the honeybee, intracellular recording reveals that neurons around the lobula and medulla region have wavelength-specific responses, such as color-opponent or narrowband responses (Kien and Menzel 1977b; Hertel 1980; Yang et al. 2004). In *D. melanogaster*, a recent study showed that photoreceptor axonal terminals inhibited each other forming a color-opponent response (Schnaitmann et al. 2018). However, no study has examined systematically whether neurons in the central nervous system have wavelength-specific response properties.

We analyzed wavelength tuning properties of the recorded neurons during the ON and OFF response phases, respectively. Tuning curves of the recorded neurons are shown in Fig. 6a, b (25 neurons are shown; the excitatory ON–OFF types whose spikes could not be detected ($n=5$) and the extra types ($n=3$) were excluded from this analysis). We quantified the response intensity using spike firing rate during the 1-s stimulus duration for the ON response (Fig. 6a) and for 1 s after the stimulus offset for the OFF response (Fig. 6b; see “Materials and methods”). The majority of responses were broadly tuned, and opponent-type responses were not found. Especially, it is rare that a neuron showed mixed excitatory and inhibitory responses to the different wavelength range matched with the photoreceptor's peak sensitivity as found in honey bees (Kien and Menzel 1977b; Yang et al. 2004). We quantified the tuning breadth of these responses using lifetime sparseness. The distribution of tuning curves was biased to broad tuning (Fig. 6c, d). However, several neurons revealed wavelength-specific responses: an excitatory ON neuron (ON_6) showed higher spike increase only in the UV range (300–375 nm, Fig. 6a); an excitatory ON–OFF type neuron (ON–OFF_3) showed higher spike firing in the middle wavelength range (425–575 nm) only at OFF response (Figs. 2b, 6b). An inhibitory type neuron showed an inhibitory response in a broad wavelength range (300–575 nm) but a slight spike increase at 625 nm during the ON response (Figs. 4a, 6a).

Wavelength separation at the population level

Since our recordings found no clear color-opponent axes at the level of these neurons, we examined how wavelength information is separated by the population level of the recorded neurons and which neurons contribute to these

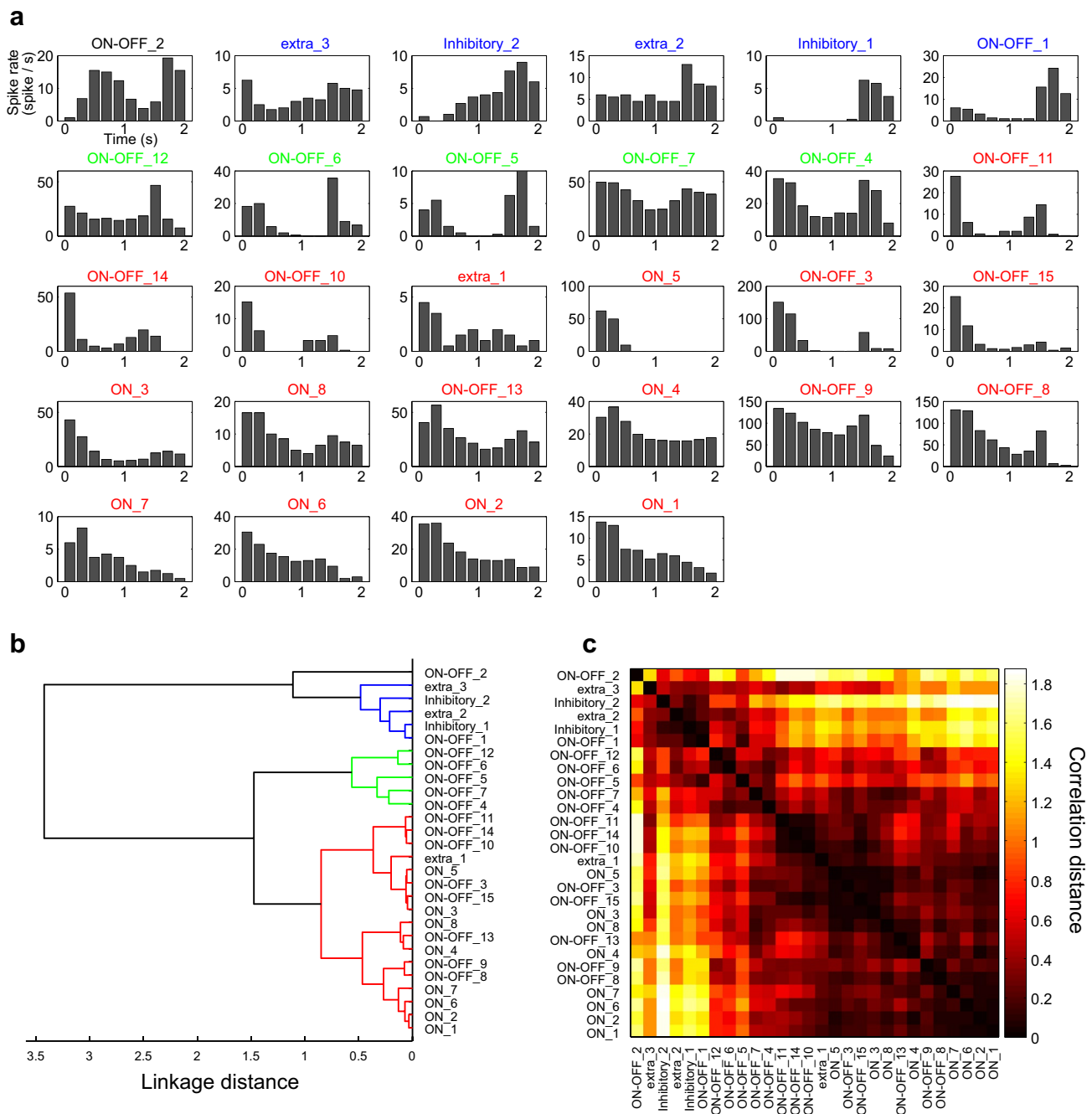


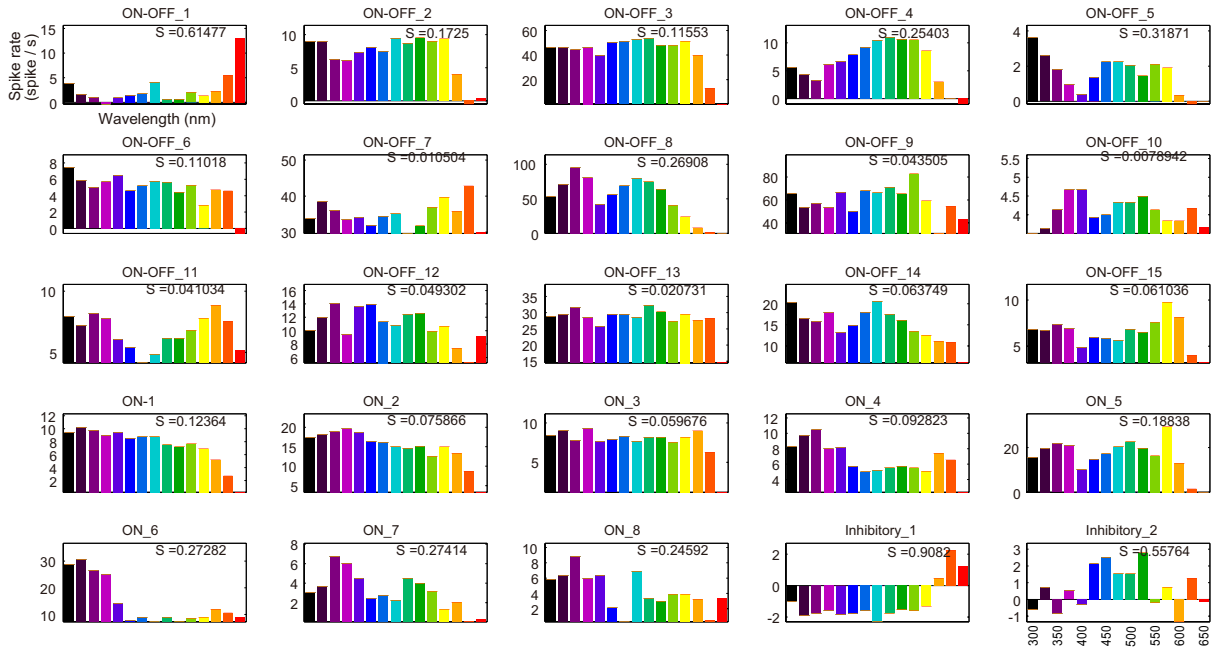
Fig. 5 Quantitative evaluation of the classification of the response types. **a** Average PSTHs calculated from the responses to the six wavelength stimuli (350, 375, 425, 475, 525, 625 nm) represent each neuron’s typical response pattern using 200 ms bins. The PSTHs are arranged from left to right and top to bottom based on the same order revealed by the cluster analysis in **(b)**. **b** Hierarchical cluster analysis

for 28 recorded neurons based on the correlation distances between the PSTHs. The cut-off threshold is set at one linkage distance, detecting three groups of separately clustered neurons colored in blue, green, and red. **c** A complete correlation matrix for 28 neurons based on the similarities of the PSTHs among each neuron. Each axis of the matrix is ordered as in **(b)**

representations. PCA was performed for the 15 wavelengths (300–650 nm by 25 nm steps) based on the response intensities either at the ON or OFF phases from the 25 recorded neurons. As shown in Fig. 7a, b, the wavelengths were separated into three groups based on ON responses (Fig. 7a) and

OFF responses (Fig. 7b). Weights (factor loadings) of each neuron for PC1 and PC2 are shown in Fig. 7c, d. Using the response intensity of the ON phase, PC1 accounting for the variance of 49.2% segregated longer wavelength (600–650 nm) to the others (300–575 nm). This can be

a ON-response



b OFF-response

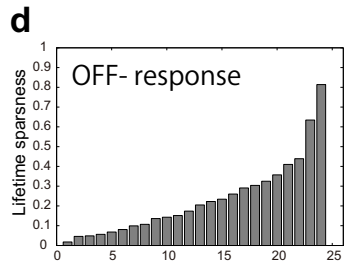
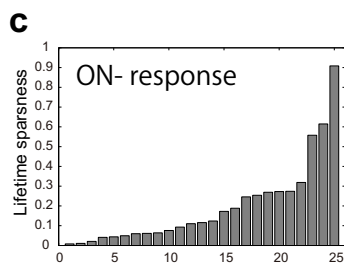
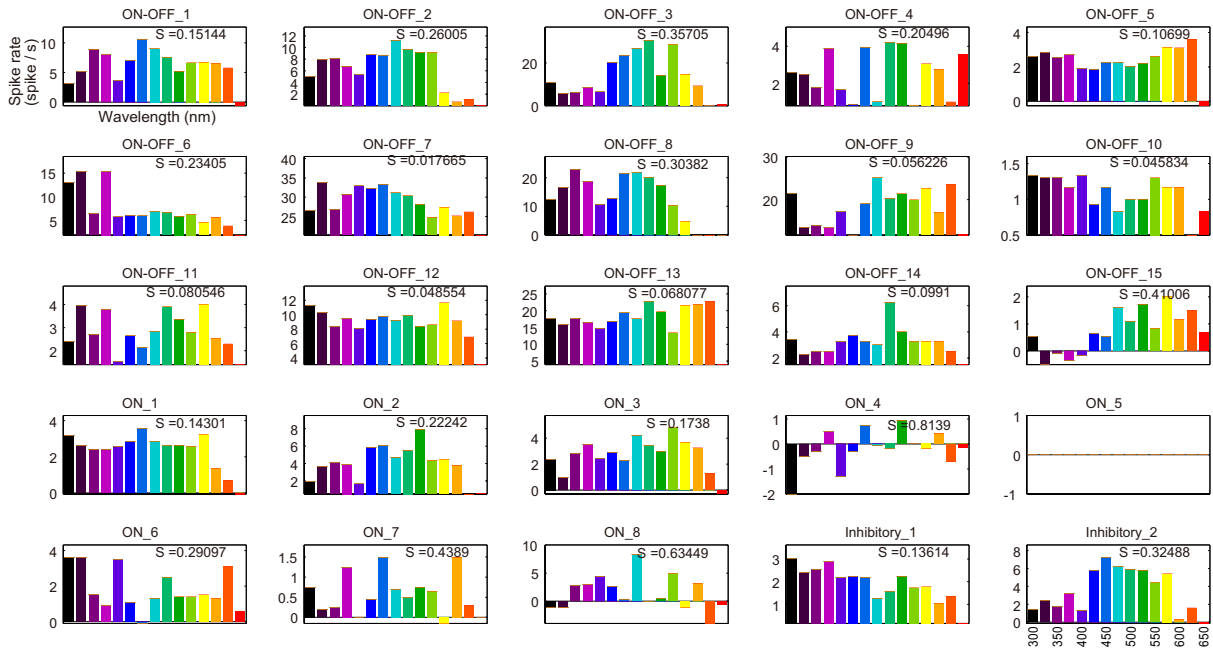


Fig. 6 Tuning breadths of 25 recorded neurons. **a, b** Tuning curves for ON responses (**a**) and OFF responses (**b**) of the 25 recorded neurons to the 15 wavelength stimuli. The value of lifetime sparseness is indicated in each graph. **c, d** Distribution of the lifetime sparseness values for ON (**c**) and OFF response (**d**)

explained by the fact that many neurons show a response decline around 600 nm, and the PC1 is sensitive to the response amplitude (Fig. 7c). PC2, accounting for 16.8% variance, further separated the UV range (300–375 nm) from the middle wavelength range (400–575 nm). The weights for the PC2 indicated that the neurons with different specificity for the UV range and middle wavelength range contributed to this separation. For example, ON–OFF_11, ON_4, and ON_6 neurons showed more intense responses in the UV range than in the middle wavelength range (Fig. 6a) and contributed to the positive direction of the PC2 axis (Fig. 7c), whereas ON–OFF_4 and inhibitory_2 neurons that showed preference for the middle wavelength range (Fig. 6a) contributed to the negative direction of the PC2 axis (Fig. 7c). Using the response intensity of the OFF phase, a similar separation was observed (Fig. 7b). PC1, accounting for 35.0% variance, separated the long wavelength range (625–650 nm) from the other wavelengths (Fig. 7b) as PC1 is sensitive to the response amplitude (Fig. 7d). PC2, accounting for 16.6% variance, further separated the UV range (300–400 nm) from the middle wavelength range (425–600 nm). Compared with the ON response representation, a 25-nm wavelength shift was observed: 400 nm is close to the UV range (300–375 nm), and 600 nm is between the middle (425–575 nm) and long (625–650 nm) wavelength ranges. As seen in the ON response, neurons that respond more strongly to UV wavelengths than to middle wavelengths contributed to the negative direction of the PC2 axis (Figs. 6b, 7d; ON–OFF_6, ON_6, Inhibitory_1) and vice versa for neurons that contributed to the positive direction of the PC2 axis (Figs. 6b, 7d; ON–OFF_15, ON_4).

Morphological identification of the neurons

In this study, cell bodies of neurons were randomly targeted in the region between the optic lobe and central brain at the posterior surface of the brain, partly including the lateral cell body region defined by Otsuna and Ito (2006). This region includes lobula columnar neurons, lobula tangential neurons, lobula plate tangential neurons, and many other kinds of neurons (Fischbach and Dittrich 1989; Otsuna and Ito 2006). Our initial attempts to target neurons using GAL4 lines that specifically label lobula columnar neurons (Panser et al. 2016) and lobula tangential neurons (Otsuna and Ito 2006) have failed. This is partly due to the small size of the cell bodies for the lobula columnar neurons and the small number of target neuron (usually one) labeled by the GAL4

lines for the lobula tangential neurons. In later-stage experiments, we performed a morphological identification of the neurons by intracellular staining during recording. Some neurons were successfully stained ($n = 3$ completely stained, $n = 4$ partially stained/10 trials). Those neurons include a lobula tangential cell and two lobula plate tangential cells (Fig. 8). The lobula tangential neuron innervates densely in the proximal lobula (lobula layer ~4–6) and projects to the anterior ventrolateral protocerebrum (Fig. 8a–d). From the morphological characteristics, this neuron is similar to lobula tangential 11 (LT11). However, its cell body position was at the posterior surface of the brain, whereas that of LT11 is reported at the dorsocentral region; moreover, its dendrites innervated more proximal than those of LT11 [LT11 innervates layers 3–5, (Otsuna and Ito 2006)]. This type of lobula tangential neuron was likely not described in detail in previous studies. This neuron is an excitatory ON type (ON_8), which showed relatively stronger excitatory responses in the UV range than other wavelengths.

Two other neurons (ON–OFF_7 and ON–OFF_14) are lobula plate tangential cells: the former is identified as a horizontal system (HS) cell (Fig. 8e, f) and the latter is similar to HS cells (wide dendritic branching in the lobula plate and axon branching in the posterior slope), but the axon extended dorsally from the posterior slope (data not shown). Among partially stained neurons, one neuron (ON–OFF_13) had a branching in the superior medial protocerebrum, and another neuron (ON_7) innervated the lateral protocerebrum and the peripheral region of the peduncle (data not shown). These results indicate that our recording targeted at least in part lobula and lobula plate neurons as well as neurons innervating the central brain. The precise morphological identification and assigning of physiological response properties to those neurons represent important future tasks.

Discussion

Chromatic properties of higher visual neurons in *D. melanogaster* were characterized in vivo using whole-cell patch-clamp recordings. The neurons were classified based on response polarities and temporal response components. The majority of neurons showed broadband tuning, and some neurons contributed to wavelength separation between UV and middle wavelength ranges.

General response patterns and their functional relevance

We classified the recorded neurons into three groups: excitatory ON–OFF, excitatory ON, and inhibitory response types. These differences in excitatory–inhibitory and light ON–OFF responses were reported in the

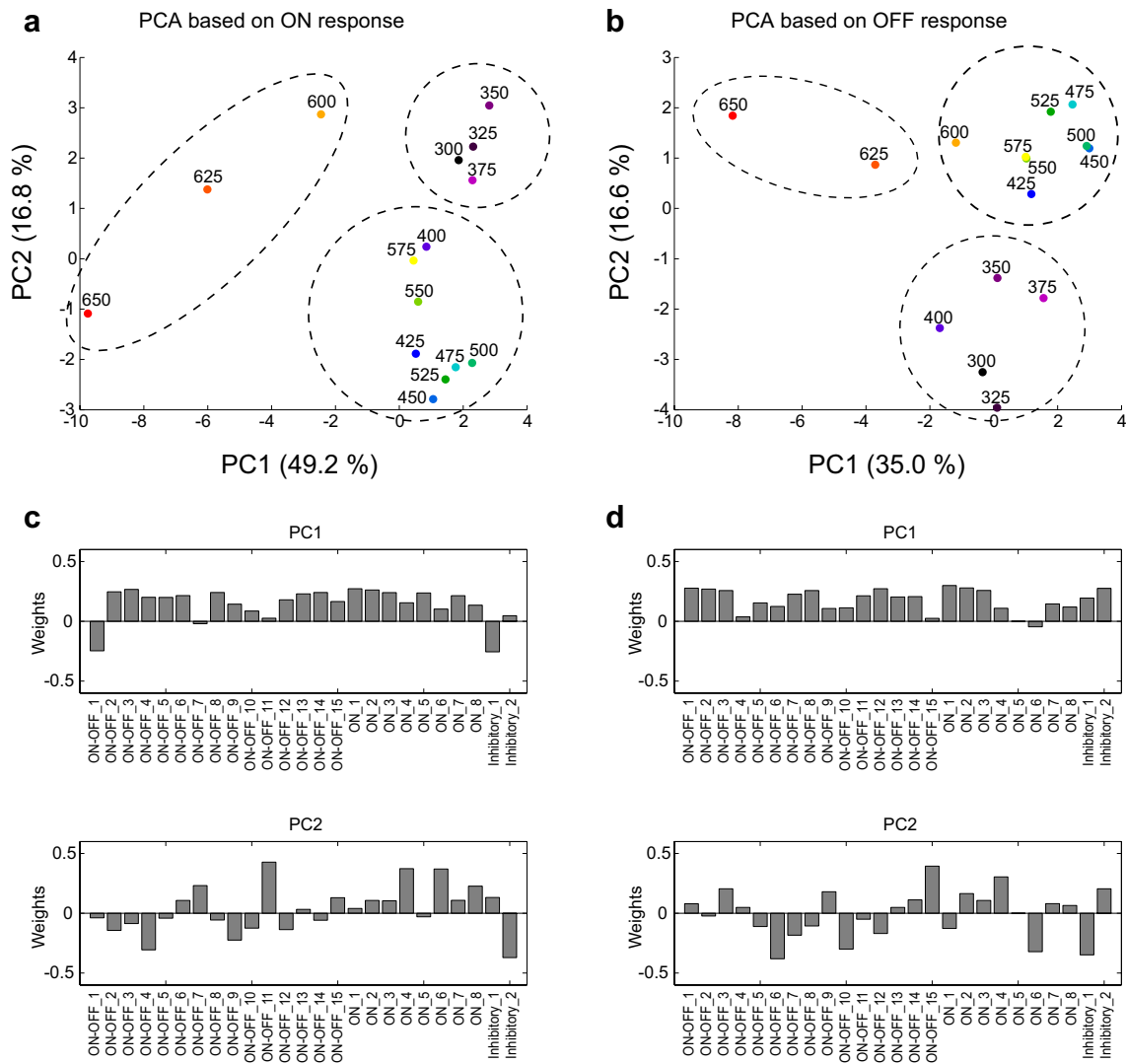


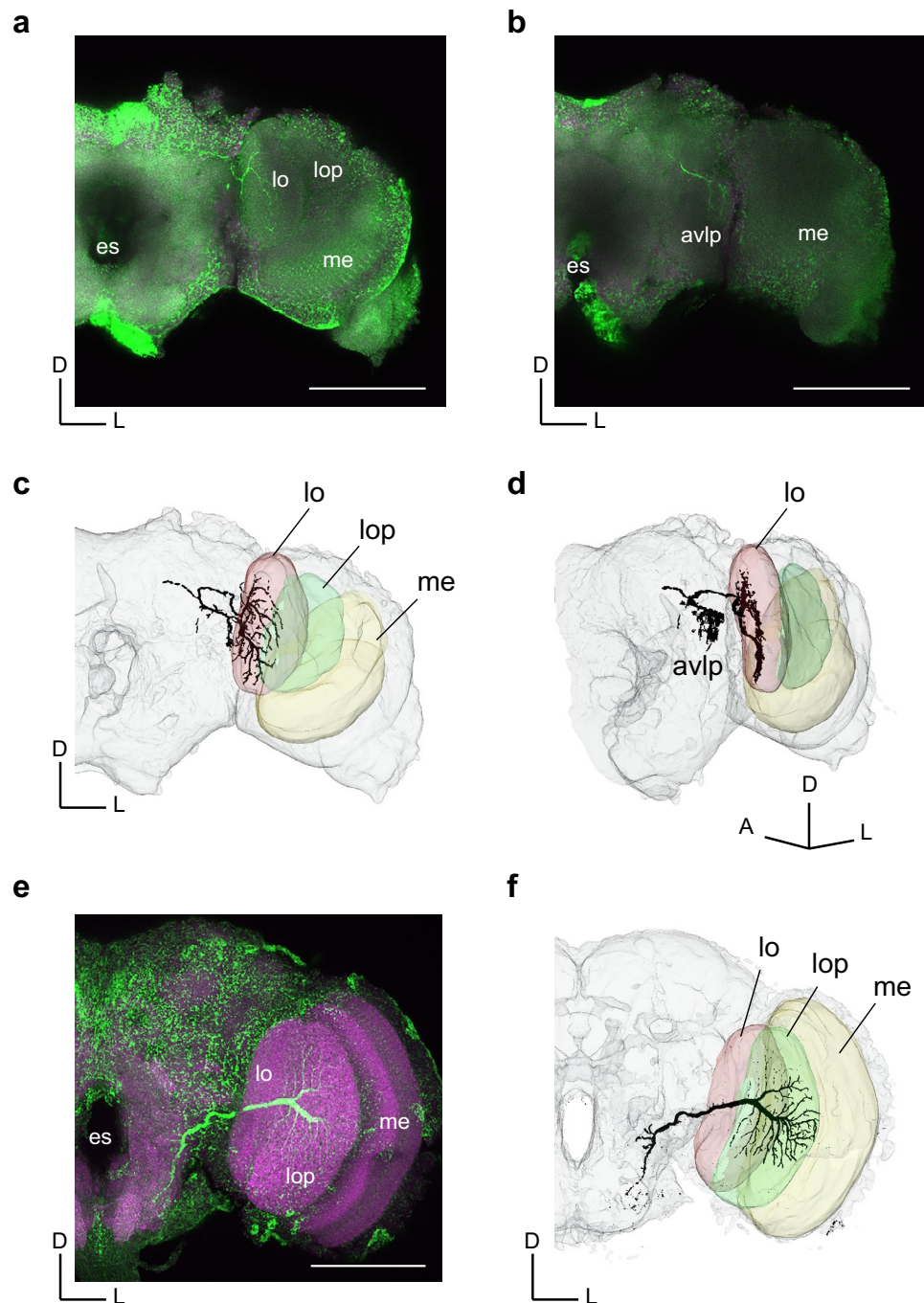
Fig. 7 Principal component analysis (PCA) reveals wavelength separation at the population level. **a**, **b** PCA for 15 wavelengths based on the response intensities of 25 recorded neurons for ON (**a**) and OFF

(**b**) response. Dotted circles visualize one of the three clustering patterns obtained by k-means clustering ($k=3$). **c**, **d** Weights (factor loadings) of PC1 and PC2 for ON (**c**) and OFF response (**d**)

electrophysiological studies to chromatic stimuli in bees, where ON-effect, sustained, OFF-effect components were described (Kien and Menzel 1977a, b; Hertel 1980; Yang et al. 2004; Paulk et al. 2009a). In flies, electrophysiological investigation for the central visual system has mainly focused on motion detection circuits. R1–6 neurons synapse with lamina neurons L1, L2, L3 and through medulla neurons Mi1, Tm3, Tm1, Tm2 to T4, T5 columnar neurons to the lobula plate tangential neurons (Behnia and Desplan 2015). Some neurons were tested with flicker stimuli in addition to motion stimuli and showed ON–OFF responses and phasic–tonic components (Douglass and Strausfeld 1995, 1996). In the motion detection system, ON-edge and OFF-edge motion stimuli are segregated early into the L1 and L2 pathways, conveyed by R1–6 photoreceptor neurons

projecting to the lamina (Joesch et al. 2010). Patch-clamp recordings of Mi1 and Tm3 (L1 pathway) and Tm1 and Tm2 (L2 pathway) demonstrate that Mi1 and Tm3 show an excitatory response to light ON, whereas Tm1 and Tm2 show an inhibitory response to light ON and an excitatory response to light OFF (Behnia et al. 2014). In contrast, R7–8 photoreceptor neurons send axons to the medulla, bypassing the lamina, but the physiological response properties of candidate second-order neurons, such as Tm5a–c, Tm20, and Tm9, for light ON and OFF are not known. Further studies should precisely identify the response polarities and temporal patterns of the neurons underlying color processing pathways at the level of second- and third-order neurons. This is important for understanding how neural response patterns are generated in higher visual neurons.

Fig. 8 Morphology of the identified neurons. **a, b** Projection images (single neuron: green, nc82: magenta) of a lobula tangential neuron (ON_8), indicating dendritic arborization in the lobula (lo) (**a**; thickness of projection = 17.68 μm) and axonal arborization in the anterior ventrolateral protocerebrum (avlp) (**b**; thickness of projection = 15.64 μm). **c, d** Three-dimensional reconstruction of the neuron from posterior view (**c**) and oblique view (**d**). **e** Projection image (thickness of projection = 23.8 μm) of the lobula plate tangential neuron (HS cell; ON-OFF_7), indicating dendritic arborization in the lobula plate (lop). **f** Three-dimensional reconstruction of the neuron from posterior view. All scale bars = 100 μm . The cell bodies of these neurons were removed with the electrode when pulling out the electrode after recording. avlp, anterior ventrolateral protocerebrum. es, esophagus. lo, lobula. lop, lobula plate. me, medulla. D, dorsal. L, lateral. A, anterior



Although we characterized detailed chromatic response properties of higher visual interneurons, these neurons are not necessarily responsible for chromatic information processing. Actually, many recorded neurons showed a rather broadband tuning that could indicate a role in achromatic processing. To establish further functional identification, our recorded neurons need to be tested with other types of stimuli, such as grating motion and moving objects. Mu et al. used *in vivo* patch-clamp recording in *D. melanogaster* and examined lobula columnar neurons and other higher brain

neurons using motion pattern and static grating stimuli (Mu et al. 2012). These kinds of stimuli should be combined with our approach. Furthermore, we employed 1-s flashing light stimuli to the entire field of the compound eye. Although many studies demonstrated that receptive fields were not relevant in the insect visual system for chromatic processing (Kien and Menzel 1977a, b; Hertel 1980; Yang et al. 2004) compared with the primate (e.g., midget ganglion cells responsible for L–M color-opponent neurons), the possibility remains that color-opponent properties related to specific

receptive fields could not be detected. Having established stable recording methods in this study, future studies might improve stimuli for which both wavelength and receptive field can be controlled.

Spectral tuning of higher visual neurons

Initial extensive studies in bees performed around the 1970s–1980s demonstrated that the honeybee has a trichromatic vision similar to primates, consisting of UV, blue, and green channels (Menzel and Backhaus 1989). Electrophysiological recordings from the medulla, lobula, and higher brain regions showed that there are broadband, narrowband, and color-opponent neurons (Erber and Menzel 1977; Kien and Menzel 1977a, b; Hertel 1980; Riehle 1981; Hertel and Maronde 1987). A color coding model was established based on these color-opponent neurons (Backhaus 1991). Relatively recent studies in honeybees and bumblebees provide additional evidence that there are many variations with the combination of color opponency, and color and motion information might be separated in different layers and pathways (Yang et al. 2004; Paulk et al. 2009a, b).

In contrast, there are only a few studies trying to examine chromatic response properties in *D. melanogaster* (Vogt et al. 2016; Schnaitmann et al. 2018; Heath et al. 2019). In our study, we characterized detailed spectral response properties of higher visual neurons using monochromatic stimuli ranging from 300 to 650 nm with 25-nm steps. Our results showed that the majority of neurons respond to a wide range of wavelengths (Fig. 6), which could be categorized as broadband neurons in the previous definition (Kien and Menzel 1977a; Yang et al. 2004). Among the five photoreceptors expressed in the compound eye, only Rh1 has a broadband sensitivity showing a sensitivity curve with two peaks at the UV (~355 and 370 nm) and cyan (~478 nm) range (Fig. 1b) (Salcedo et al. 1999). However, the tuning curves of our recorded broadband type neurons show a flatter shape compared to Rh1's bi-modal curve. This difference suggests that the broadband responses are not solely dominated by the Rh1 input, but interacted with other inputs from narrow band photoreceptors (Rh3–Rh6) or these narrow band inputs could be combined to generate the broadband tuning. Gap junctions between different photoreceptor classes could contribute to these interactions (Wardill et al. 2012). Other possibility is that there is a kind of gain control mechanism, in which stronger input is suppressed and weaker input is enhanced, through the processing stages of the visual circuits. This possibility is partly supported by the observation that many neurons displayed certain level of responses at the 600–650 nm range (Fig. 6), where the spectral sensitivities of even longer wavelength sensitive photoreceptors (Rh6 and Rh1) are very low (Fig. 1b). On the other hand, typical color-opponent-type

responses found in bees were not identified. Instead, we found that two ranges of wavelengths, UV (300–375 nm) and middle wavelength (425–575 nm) ranges were separated at the population level of the recorded neurons owing to neurons that have wavelength-specific tuning either in the UV range or middle wavelength range (Fig. 7). In recent studies, color opponency was discovered in *D. melanogaster* at the axon terminals of R7 and R8 photoreceptors within the same ommatidia (Schnaitmann et al. 2018) and between neighboring ommatidia via horizontal cell-like Dm9 neurons (Heath et al. 2019). Interestingly, UV-blue and UV-green opponency is the main component of the color opponency formed by the reciprocal inhibition between R7 and R8 within the same ommatidium, which leads to a high-resolution chromatic pathway. UV vs middle wavelength contrast could be enhanced by these color-opponent mechanisms at the medulla and transmitted to the downstream neurons, which might reflect in the UV or middle wavelength range preference found in our recordings.

Identification of neurons and chromatic pathways

In this study, three neurons (two lobula plate tangential neurons and one lobula tangential neuron) were identified (Fig. 8). Both lobula plate tangential neurons were excitatory ON–OFF type (ON–OFF_7, ON–OFF_14) having relatively broadband tuning (Fig. 6). Among the excitatory ON–OFF type neurons, there are variations in firing duration (Table 1, Fig. 2), amplitude and time course of firing (Fig. 5), and spectral tuning (Fig. 6). Therefore, all the ON–OFF neurons should not be the lobula plate tangential neurons but include different types of neurons. Conversely, the excitatory ON neurons represent likely a continuum with some of the excitatory ON–OFF type neurons (Fig. 5), there might be a possibility that a part of the both types of neurons belong to the same type of neurons. In addition, we succeeded in recording from a lobula tangential neuron that is an excitatory ON type neuron and displayed a stronger excitatory response in the UV range than in the middle wavelength range (Fig. 6a). This neuron arborized in the proximal lobula (lo layer ~4–6) and projected to the anterior ventrolateral protocerebrum, similar to LT11 morphological characteristics (Fig. 8a–d). LT11 receives inputs from Tm5a-c neurons at the lobula layer 5 and projects to the ventrolateral protocerebrum (Otsuna and Ito 2006; Lin et al. 2016). LT11 is also suggested to play a role in wavelength-dependent phototaxis (Otsuna et al. 2014). The neuron which we stained was of a different LT type, but could be an important neuron for chromatic processing. In addition to the lobula pathway, a previous study found that the medulla neurons that convey chromatic information directly to the mushroom body accessory calyx (Vogt et al. 2016). The recordings from γ d-KCs showed excitatory responses both to green and blue light.

How blue and green information is separated at this level is not characterized. Future studies should address how chromatic information is processed in these parallel pathways and what neural mechanisms are used for color vision underlying true color vision and spectral preference.

D. melanogaster becomes a prominent model for systematically understanding the neural mechanisms for color vision (Behnia and Desplan 2015; Song and Lee 2018). Although our neuron sample is very small compared with the total number of neurons in this region, our study provides a first mapping of chromatic response properties of single neurons in the higher visual center. Multidisciplinary approaches combining our approach with genetic manipulation, imaging, and behavioral experiments will help to resolve color processing mechanisms in this important model organism, providing crucial insights into how animals see color in general.

Acknowledgements We would like to thank the members of Yamauchi Laboratory for valuable comments and Ms. Hiromi Usui for technical support. This work was supported by JSPS KAKENHI Grant Numbers JP25870768, JP18K06342. The authors declare no competing financial interest.

Compliance with ethical standards

Conflict of interest The authors declare that they have no conflict of interest.

References

- Arikawa K, Stavenga DG (2014) Insect photopigments: photoreceptor spectral sensitivities and visual adaptations. In: Hunt DM, Hankins MW, Collin SP, Marshall NJ (eds) Evolution of visual and non-visual pigments. Springer, Boston, pp 137–162
- Arikawa K, Mizuno S, Kinoshita M, Stavenga DG (2003) Coexpression of two visual pigments in a photoreceptor causes an abnormally broad spectral sensitivity in the eye of the butterfly *Papilio xuthus*. *J Neurosci* 23:4527–4532
- Backhaus W (1991) Color opponent coding in the visual system of the honeybee. *Vis Res* 31:1381–1397
- Behnia R, Desplan C (2015) Visual circuits in flies: beginning to see the whole picture. *Curr Opin Neurobiol* 34:125–132. <https://doi.org/10.1016/j.conb.2015.03.010>
- Behnia R, Clark DA, Carter AG, Clandinin TR, Desplan C (2014) Processing properties of ON and OFF pathways for *Drosophila* motion detection. *Nature* 512:427–430. <https://doi.org/10.1038/nature13427>
- Conway BR, Chatterjee S, Field GD, Horwitz GD, Johnson EN, Koida K, Mancuso K (2010) Advances in color science: from retina to behavior. *J Neurosci* 30:14955–14963. <https://doi.org/10.1523/JNEUROSCI.4348-10.2010>
- Dacey DM, Packer OS (2003) Colour coding in the primate retina: diverse cell types and cone-specific circuitry. *Curr Opin Neurobiol* 13:421–427
- Douglass JK, Strausfeld NJ (1995) Visual motion detection circuits in flies: peripheral motion computation by identified small-field retinotopic neurons. *J Neurosci* 15:5596–5611
- Douglass JK, Strausfeld NJ (1996) Visual motion-detection circuits in flies: parallel direction- and non-direction-sensitive pathways between the medulla and lobula plate. *J Neurosci* 16:4551–4562
- Erber J, Menzel R (1977) Visual interneurons in the median protocerebrum of the bee. *J Comp Physiol A* 121:65–77
- Fischbach K (1979) Simultaneous and successive colour contrast expressed in “slow” phototactic behaviour of walking *Drosophila melanogaster*. *J Comp Physiol A* 130:161–171
- Fischbach K-F, Dittrich A (1989) The optic lobe of *Drosophila melanogaster*. I. A Golgi analysis of wild-type structure. *Cell Tissue Res* 258:441–475
- Gao S et al (2008) The neural substrate of spectral preference in *Drosophila*. *Neuron* 60:328–342. <https://doi.org/10.1016/j.neuron.2008.08.010>
- Gegenfurtner KR, Kiper DC (2003) Color vision. *Annu Rev Neurosci* 26:181–206. <https://doi.org/10.1146/annurev.neuro.26.041002.131116>
- Heath SL, Christenson MP, Oriol E, Saavedra-Weisenhaus M, Kohn JR, Behnia R (2019) Circuit mechanisms underlying chromatic encoding in *Drosophila* photoreceptors. *bioRxiv:790295* <https://doi.org/10.1101/790295>
- Hempel de Ibarra N, Vorobyev M, Menzel R (2014) Mechanisms, functions and ecology of colour vision in the honeybee. *J Comp Physiol A* 200:411–433. <https://doi.org/10.1007/s00359-014-0915-1>
- Hertel H (1980) Chromatic properties of identified interneurons in the optic lobes of the bee. *J Comp Physiol A* 137:215–231
- Hertel H, Maronde U (1987) The physiology and morphology of centrally projecting visual interneurons in the honeybee brain. *J Exp Biol* 133:301–315
- Hu KG, Stark WS (1977) Specific receptor input into spectral preference in *Drosophila*. *J Comp Physiol A* 121:241–252
- Jacob K, Willmund R, Folkers E, Fischbach K, Spatz HC (1977) T-maze phototaxis of *Drosophila melanogaster* and several mutants in the visual systems. *J Comp Physiol A* 116:209–225
- Jagadeish S, Barnea G, Clandinin TR, Axel R (2014) Identifying functional connections of the inner photoreceptors in *Drosophila* using Tango-Trace. *Neuron* 83:630–644. <https://doi.org/10.1016/j.neuron.2014.06.025>
- Joesch M, Schnell B, Raghu SV, Reiff DF, Borst A (2010) ON and OFF pathways in *Drosophila* motion vision. *Nature* 468:300–304. <https://doi.org/10.1038/nature09545>
- Kelber A (2016) Colour in the eye of the beholder: receptor sensitivities and neural circuits underlying colour opponency and colour perception. *Curr Opin Neurobiol* 41:106–112. <https://doi.org/10.1016/j.conb.2016.09.007>
- Kelber A, Vorobyev M, Osorio D (2003) Animal colour vision-behavioural tests and physiological concepts. *Biol Rev* 78:81–118. <https://doi.org/10.1017/s1464793102005985>
- Kien J, Menzel R (1977a) Chromatic properties of interneurons in the optic lobes of the bee. I. Broad band neurons. *J Comp Physiol A* 113:17–34
- Kien J, Menzel R (1977b) Chromatic properties of interneurons in the optic lobes of the bee. II. Narrow band and colour opponent neurons. *J Comp Physiol A* 113:35–53
- Kinoshita M, Arikawa K (2000) Colour constancy in the swallowtail butterfly *Papilio xuthus*. *J Exp Biol* 203:3521–3530
- Kinoshita M, Arikawa K (2014) Color and polarization vision in foraging *Papilio*. *J Comp Physiol A* 200:513–526. <https://doi.org/10.1007/s00359-014-0903-5>
- Kinoshita M, Takahashi Y, Arikawa K (2008) Simultaneous color contrast in the foraging swallowtail butterfly, *Papilio xuthus*. *J Exp Biol* 211:3504–3511. <https://doi.org/10.1242/jeb.017848>
- Krauskopf J, Williams DR, Heeley DW (1982) Cardinal directions of color space. *Vis Res* 22:1123–1131. [https://doi.org/10.1016/0042-6989\(82\)90077-3](https://doi.org/10.1016/0042-6989(82)90077-3)

- Lin TY, Luo J, Shinomiya K, Ting CY, Lu Z, Meinertzhagen IA, Lee CH (2016) Mapping chromatic pathways in the *Drosophila* visual system. *J Comp Neurol* 524:213–227. <https://doi.org/10.1002/cne.23857>
- Mazzoni EO et al (2008) Iroquois complex genes induce co-expression of rhodopsins in *Drosophila*. *PLoS Biol* 6:e97. <https://doi.org/10.1371/journal.pbio.0060097>
- Melnattur KV, Pursley R, Lin TY, Ting CY, Smith PD, Pohida T, Lee CH (2014) Multiple redundant medulla projection neurons mediate color vision in *Drosophila*. *J Neurogenet* 28:374–388. <https://doi.org/10.3109/01677063.2014.891590>
- Menzel R, Backhaus W (1989) Color vision honey bees: phenomena and physiological mechanisms. In: Stavenga DG, Hardie RC (eds) *Facets of vision*. Springer, Berlin, Heidelberg, pp 281–297
- Morante J, Desplan C (2008) The color-vision circuit in the medulla of *Drosophila*. *Curr Biol* 18:553–565. <https://doi.org/10.1016/j.cub.2008.02.075>
- Mu L, Ito K, Bacon JP, Strausfeld NJ (2012) Optic glomeruli and their inputs in *Drosophila* share an organizational ground pattern with the antennal lobes. *J Neurosci* 32:6061–6071. <https://doi.org/10.1523/JNEUROSCI.0221-12.2012>
- Neumeyer C (1980) Simultaneous color contrast in the honeybee. *J Comp Physiol A* 139:165–176
- Neumeyer C (1981) Chromatic adaptation in the honeybee: successive color contrast and color constancy. *J Comp Physiol A* 144:543–553
- Otsuna H, Ito K (2006) Systematic analysis of the visual projection neurons of *Drosophila melanogaster*. I. Lobula-specific pathways. *J Comp Neurol* 497:928–958. <https://doi.org/10.1002/cne.21015>
- Otsuna H, Shinomiya K, Ito K (2014) Parallel neural pathways in higher visual centers of the *Drosophila* brain that mediate wavelength-specific behavior. *Front Neural Circuits* 8:8. <https://doi.org/10.3389/fncir.2014.00008>
- Panser K, Tirian L, Schulze F, Villalba S, Jefferis GS, Buhler K, Straw AD (2016) Automatic segmentation of *Drosophila* neural compartments using GAL4 expression data reveals novel visual pathways. *Curr Biol* 26:1943–1954. <https://doi.org/10.1016/j.cub.2016.05.052>
- Paulk AC, Phillips-Portillo J, Dacks AM, Fellous JM, Gronenberg W (2008) The processing of color, motion, and stimulus timing are anatomically segregated in the bumblebee brain. *J Neurosci* 28:6319–6332. <https://doi.org/10.1523/JNEUROSCI.1196-08.2008>
- Paulk AC, Dacks AM, Gronenberg W (2009a) Color processing in the medulla of the bumblebee (Apidae: *Bombus impatiens*). *J Comp Neurol* 513:441–456. <https://doi.org/10.1002/cne.21993>
- Paulk AC, Dacks AM, Phillips-Portillo J, Fellous JM, Gronenberg W (2009b) Visual processing in the central bee brain. *J Neurosci* 29:9987–9999. <https://doi.org/10.1523/JNEUROSCI.1325-09.2009>
- Riehle A (1981) Color opponent neurons of the honeybee in a heterochromatic flicker test. *J Comp Physiol A* 142:81–88
- Salcedo E, Huber A, Henrich S, Chadwell LV, Chou WH, Paulsen R, Britt SG (1999) Blue- and green-absorbing visual pigments of *Drosophila*: ectopic expression and physiological characterization of the R8 photoreceptor cell-specific Rh5 and Rh6 rhodopsins. *J Neurosci* 19:10716–10726
- Salomon CH, Spatz H-C (1983) Colour vision in *Drosophila melanogaster*: wavelength discrimination. *J Comp Physiol A* 150:31–37
- Schnaitmann C, Garbers C, Wachtler T, Tanimoto H (2013) Color discrimination with broadband photoreceptors. *Curr Biol* 23:2375–2382. <https://doi.org/10.1016/j.cub.2013.10.037>
- Schnaitmann C, Haikala V, Abraham E, Oberhauser V, Thestrup T, Griesbeck O, Reiff DF (2018) Color processing in the early visual system of *Drosophila*. *Cell* 172(318–330):e318. <https://doi.org/10.1016/j.cell.2017.12.018>
- Seki Y, Rybak J, Wicher D, Sachse S, Hansson BS (2010) Physiological and morphological characterization of local interneurons in the *Drosophila* antennal lobe. *J Neurophysiol* 104:1007–1019. <https://doi.org/10.1152/jn.00249.2010>
- Solomon SG, Lennie P (2007) The machinery of colour vision. *Nat Rev Neurosci* 8:276–286. <https://doi.org/10.1038/nrn2094>
- Song BM, Lee CH (2018) Toward a mechanistic understanding of color vision in insects. *Front Neural Circuits* 12:16. <https://doi.org/10.3389/fncir.2018.00016>
- Suzuki Y, Ikeda H, Miyamoto T, Miyakawa H, Seki Y, Aonishi T, Morimoto T (2015) Noise-robust recognition of wide-field motion direction and the underlying neural mechanisms in *Drosophila melanogaster*. *Sci Rep* 5:10253. <https://doi.org/10.1038/srep10253>
- Takemura SY, Lu Z, Meinertzhagen IA (2008) Synaptic circuits of the *Drosophila* optic lobe: the input terminals to the medulla. *J Comp Neurol* 509:493–513. <https://doi.org/10.1002/cne.21757>
- Takemura SY et al (2013) A visual motion detection circuit suggested by *Drosophila* connectomics. *Nature* 500:175–181. <https://doi.org/10.1038/nature12450>
- Venken KJ, Simpson JH, Bellen HJ (2011) Genetic manipulation of genes and cells in the nervous system of the fruit fly. *Neuron* 72:202–230. <https://doi.org/10.1016/j.neuron.2011.09.021>
- Vogt K et al (2016) Direct neural pathways convey distinct visual information to *Drosophila* mushroom bodies. *Elife*. <https://doi.org/10.7554/eLife.14009>
- Wardill TJ et al (2012) Multiple spectral inputs improve motion discrimination in the *Drosophila* visual system. *Science* 336:925–931. <https://doi.org/10.1126/science.1215317>
- Wernet MF, Mazzoni EO, Celik A, Duncan DM, Duncan I, Desplan C (2006) Stochastic spineless expression creates the retinal mosaic for colour vision. *Nature* 440:174–180. <https://doi.org/10.1038/nature04615>
- Wernet MF, Perry MW, Desplan C (2015) The evolutionary diversity of insect retinal mosaics: common design principles and emerging molecular logic. *Trends Genet* 31:316–328. <https://doi.org/10.1016/j.tig.2015.04.006>
- Willmore B, Tolhurst DJ (2001) Characterizing the sparseness of neural codes. *Network* 12:255–270
- Wilson RI, Turner GC, Laurent G (2004) Transformation of olfactory representations in the *Drosophila* antennal lobe. *Science* 303:366–370. <https://doi.org/10.1126/science.1090782>
- Yamaguchi S, Desplan C, Heisenberg M (2010) Contribution of photoreceptor subtypes to spectral wavelength preference in *Drosophila*. *Proc Natl Acad Sci USA* 107:5634–5639. <https://doi.org/10.1073/pnas.0809398107>
- Yang EC, Lin HC, Hung YS (2004) Patterns of chromatic information processing in the lobula of the honeybee, *Apis mellifera* L. *J Insect Physiol* 50:913–925. <https://doi.org/10.1016/j.jinsphys.2004.06.010>

Publisher's Note Springer Nature remains neutral with regard to jurisdictional claims in published maps and institutional affiliations.